Li *et al.*
Biotechnology for Biofuels and Bioproducts (2024) 17:130
https://doi.org/10.1186/s13068-024-02576-4

Biotechnology for Biofuels and Bioproducts

RESEARCH

Open Access

Engineering the L-tryptophan metabolism for efficient de novo biosynthesis of tryptophol in *Saccharomyces cerevisiae*

Ye Li[1*†], Jingzhen Sun[1†], Zhenhao Fu[1†], Yubing He[1], Xiaorui Chen[1], Shijie Wang[1], Lele Zhang[1,2], Jiansheng Jian[2], Weihua Yang[3], Chunli Liu[1], Xiuxia Liu[1], Yankun Yang[1] and Zhonghu Bai[1*]

Abstract

Tryptophol (IET) is a metabolite derived from L-tryptophan that can be isolated from plants, bacteria, and fungi and has a wide range of biological activities in living systems. Despite the fact that IET biosynthesis pathways exist naturally in living organisms, industrial-scale production of IET and its derivatives is solely based on environmentally unfriendly chemical conversion. With diminishing petroleum reserves and a significant increase in global demand in all major commercial segments, it becomes essential to develop new technologies to produce chemicals from renewable resources and under mild conditions, such as microbial fermentation. Here we characterized and engineered the less-studied L-tryptophan pathway and IET biosynthesis in the baker's yeast *Saccharomyces cerevisiae*, with the goal of investigating microbial fermentation as an alternative/green strategy to produce IET. In detail, we divided the aromatic amino acids (AAAs) metabolism related to IET synthesis into the shikimate pathway, the L-tryptophan pathway, the competing L-tyrosine/L-phenylalanine pathways, and the Ehrlich pathway based on a modular engineering concept. Through stepwise engineering of these modules, we obtained a yeast mutant capable of producing IET up to 1.04 g/L through fed-batch fermentation, a ~ 650-fold improvement over the wild-type strain. Besides, our engineering process also revealed many insights about the regulation of AAAs metabolism in *S. cerevisiae*. Finally, during our engineering process, we also discovered yeast mutants that accumulate anthranilate and L-tryptophan, both of which are precursors of various valuable secondary metabolites from fungi and plants. These strains could be developed to the chassis for natural product biosynthesis upon introducing heterologous pathways.

Keywords Aromatic amino acids, Ehrlich pathway, Metabolic engineering, *Saccharomyces cerevisiae*, L-Tryptophan, Tryptophol

Background

Tryptophol (indole-3-ethanol, IET) is a metabolite derived from L-tryptophan (L-Trp) that can be isolated from terrestrial and marine plants, bacteria, and fungi [1]. It demonstrates a wide range of biological activities in living organisms: (1) It acts as a growth factor in plants, inducing leaf size reduction [2]; (2) it acts as a quorum sensing (QS) molecule in quite a few microorganisms, responsible for cell–cell communication [3]; (3) It also has anti-fungal/anti-microbial/anti-viral/anti-tumor properties, e. g. inducing apoptosis of leukemia U937

†Ye Li, Jingzhen Sun and Zhenhao Fu are First authors.

*Correspondence:
Ye Li
yeli0622@jiangnan.edu.cn
Zhonghu Bai
baizhonghu@jiangnan.edu.cn
[1] Key Laboratory of Industrial Biotechnology of Ministry of Education and School of Biotechnology, Jiangnan University, Wuxi 214122, China
[2] Wuxi Tmaxtree Biotechnology Co. Ltd., Wuxi 214072, China
[3] Changxing Pharmaceutical Co. Ltd., Huzhou 313100, China

cells [4]. As a critical drug precursor, IET and its derivatives can be chemically converted into a large number of bioactive compounds of pharmaceutical importance by modifying the hydroxyethyl side chain and/or the nitrogen atom [1]. Representative compounds synthesized from IET or its derivatives include (1) furoindoline derivatives that treat glaucoma, cancer, cachexia, Castleman's disease, rheumatoid arthritis, etc. [5]; (2) antimigraine drugs of the triptan family, such as sumatriptan, rizatriptan, and zolmitriptan [6]; (3) the antiadrenergic agent indoramine [7]; (4) etodolac and derivatives with known anti-inflammatory, analgesic, anti-cancer and enzyme inhibitory properties [8]; (5) indole terpenoids, such as the ergot alkaloid lysergic acid [9]; and (6) goniomitine and carbazole-type derivatives with anti-tumor properties [10] (Fig. 1A).

Although IET biosynthesis pathways exist naturally in many living organisms, industrial-scale production of IET and its derivatives is solely based on synthetic chemistry, which benefits from flourishing indole chemistry [1, 11–14]. The most efficient method to synthesize IET and its derivative is based on the classical Fischer indole synthetic methodology [15] (Table 1). Based on this approach and through process optimization, a continuous flow synthesis of IET in a tubular reactor with a maximum conversion of 93% for the substrate phenyl hydrazine hydrochloride and an IET yield of 72% in 6 min at 155 °C was developed [15]. In a continuous microwave reactor (CMWR), further process optimization resulted in an IET yield of 95% in 5 min [15]. Another study reported an efficient and multikilogram-scale process for 7-ethyltryptophol production based on the same Fischer indole synthesis approach [16]. Within 5 min of an optimized process, ~ 100% substrate conversion and 7-ethyltryptophol yields of up to 75% were achieved at 115 °C.

Although IET's chemical synthesis is highly efficient, with diminishing petroleum reserves, there is a greater emphasis on developing new technologies to produce chemicals from renewable resources and under mild conditions, such as microbial fermentation and enzyme catalysis [17, 18]. Market analyses also predicted a significant increase in global demand in all major commercial segments, emphasizing the need to develop bio-renewable strategies and reduce the use of non-renewable resources as primary feedstocks [19]. Actually, because IET is a metabolite isolated from various organisms, researchers around the world have already attempted to produce it using microbial approaches as a bio-renewable alternative to traditional chemical synthesis. Yeast species were used as hosts to synthesize IET in several studies [20–24] due to their strong endogenous Ehrlich pathway [25], which effectively converts L-Trp to IET in three-step reactions (Table 1). In a recent study, the complicated effects of L-Trp addition on cell growth, IET production, and Ehrlich pathway gene expression were investigated in *S. cerevisiae* [24]. IET titer of up to 266 mg/L was achieved upon supplementing more than 600 mg/L L-Trp in the media. IET was also produced by non-conventional yeast species, such as *Zygosaccharomyces priorianus* (585 mg/L) [21], *Debaryomyces hansenii* (4.35 mg/L after 48 h fermentation) [20] and *Candida albicans* (1.77 mg/L after 120 h fermentation at 25 °C [20] and 3.24 mg/L after 28 h fermentation at 30 °C [23]).

In these prior studies, flux distributions and metabolic regulations regarding yeast L-Trp metabolism were rarely investigated. Supplementing the precursor L-Trp in the media (up to 2.5 g/L [24]) was required to achieve high titers, implying a low metabolic flux toward L-Trp biosynthesis in endogenous yeast metabolism. We suspected this is also why efficient de novo biosynthesis of IET from low-cost carbon sources like glucose has never been achieved. With this hypothesis in mind, here we investigated and characterized the metabolic pathways relevant to AAAs and IET synthesis in *S. cerevisiae* (Fig. 1B). We used a modular-based engineering strategy to debottleneck several rate-determining steps in the IET synthesis pathways, resulting in an engineered strain capable of solely using glucose to produce IET up to 1.04 g/L. This is a 3.9-fold increase to the natural producer with the supplementing of the precursor L-Trp [24]. Meanwhile, our engineering process also contributed to discovering many new insights into the regulation of AAAs metabolism, as well as the identification of yeast mutants that accumulate anthranilate and L-tryptophan.

Materials and methods

Materials

TaKaRa Ex Taq™ DNA polymerase and PrimeSTAR™ Max DNA Polymerase were purchased from TaKaRa Bio (Kusatsu, Shiga, Japan). Type IIS restriction enzymes *BsmBI* (*Esp3I*) and *BsaI* (*Eco31I*) were purchased from Thermo Fisher Scientific (Waltham, MA, USA). T7 DNA ligase and T4 DNA ligase buffer were purchased from New England Biolabs (Ipswich, MA, USA). All yeast codon-optimized heterologous genes were synthesized by GENEWIZ (Suzhou, Jiangsu, China). Unless otherwise specified, the chemicals used were purchased from Adamas Reagent, Ltd. (China).

Plasmids, strains and growth media

All plasmids and strains used in this study are listed in Tables S1 and S2, respectively. The main primers used in this study are listed in Table S3.

S. cerevisiae strains BY4741 (*MATa, his3Δ1, leu2Δ0, met15Δ0, ura3Δ0*) [26] and CEN.PK2-1D (*MATα ura3-52 leu2-3,112 trp1-289 his3-Δ1 MAL2-8c SUC2*)

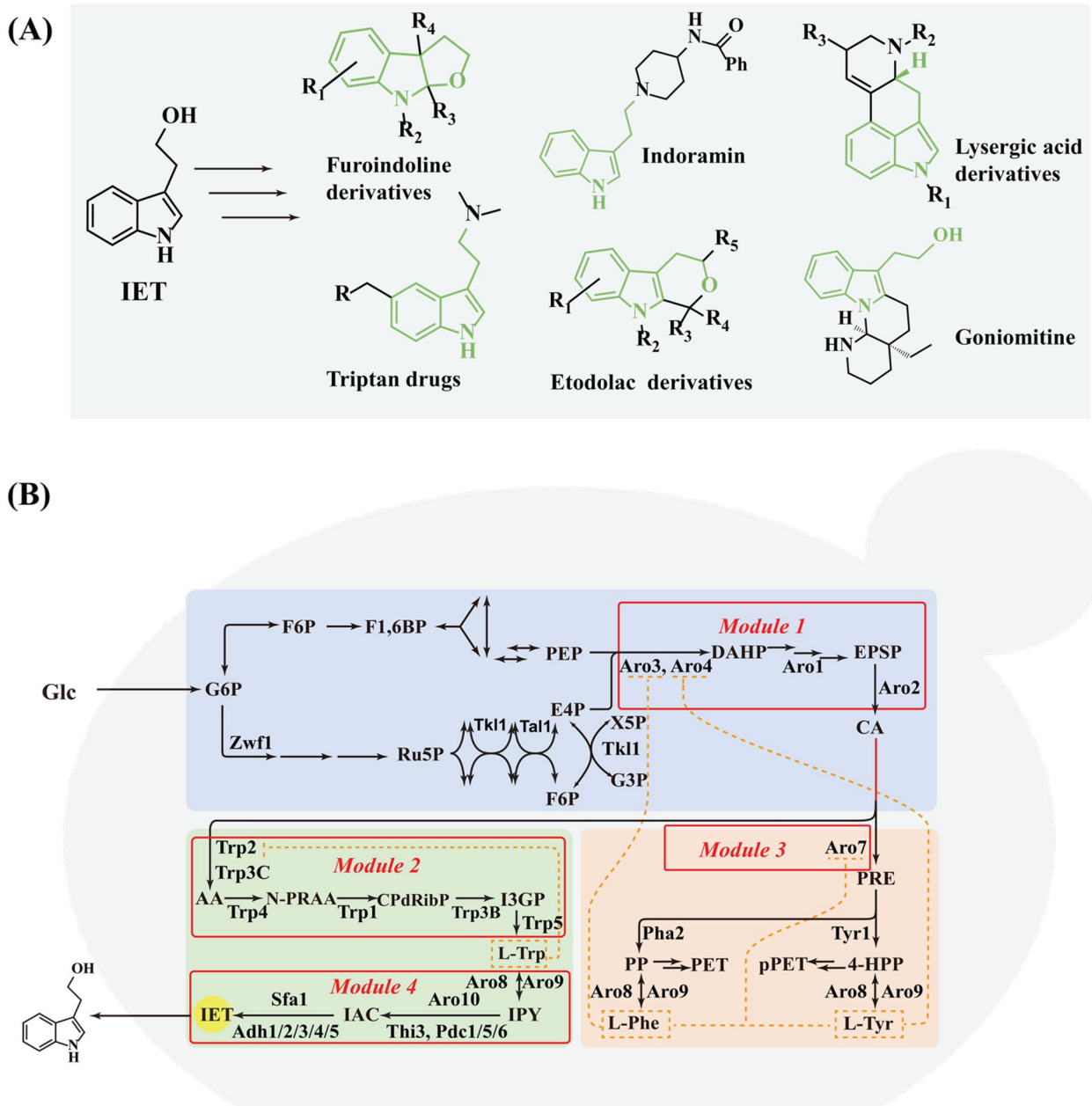

Fig. 1 Critical role of IET as a drug precursor and the metabolic pathways relating to IET biosynthesis in *S. cerevisiae*. **A** IET can be converted into many drugs. Bonds and atoms in green indicate the backbone of IET within the derived compounds. R, R1, R2, R3, or R5 donates a side chain group attached to the rest of a molecule. **B** Pathways relating to AAAs metabolism and IET biosynthesis are divided into four modules, comprehensively characterized and engineered in this study. Module 1, shikimate pathway; Module 2, L-tryptophan synthesis pathway; Module 3, the competing pathway relating to the synthesis of L-phenylalanine and L-tyrosine; Module 4, the Ehrlich pathway. Dashed lines indicate feedback inhibitions at the enzyme level

[27] were used as parent strains to construct genetically engineered strains to produce IET or Me-AA. BY4741 stock was prepared and propagated in 1% YPD medium (1% yeast extract, 2% peptone, 2% glucose) at 30 °C. *E. coli* JM109 was used to construct plasmids. Plasmid-harboring *E. coli* was cultured at 37 °C using LB medium (1% tryptone, 0.5% yeast extract, and 1% NaCl), supplemented with chloramphenicol, ampicillin, or kanamycin. The concentrations of antibiotics were 25 mg/L for chloramphenicol, 100 mg/L for ampicillin, and 50 mg/L for kanamycin, respectively.

Table 1 Summary of (substituted) IET produced by chemical and microbial approaches

Method	Product	Substrates/precursors	Conditions	Yield/titer	References
Chemical conversion (Fischer indole synthesis)	IET	Phenyl hydrazine hydrochloride, 2,3-dihydrofuran	Continuous microwave reactor, 5 min, 155 °C	95%	[15]
	7-Ethyltryptophol	2-Ethylphenylhydrazine, 4-hydroxybutyraldehyde	Continuous flow reactor, 5 min, 115 °C	75%	[16]
Microbial fermentation	IET	Glucose + L-Trp	*Candida albicans*, shake flask, 30°C, 28 h	3.24 mg/L	[23]
		Glucose + L-Trp	*C. albicans*, shake flask, 25°C, 120 h	1.77 mg/L	[20]
		Glucose + L-Trp	*Debaryomyces hansenii* shake flask, 25°C, 48 h	4.35 mg/L	[20]
		Glucose + L-Trp	*S. cerevisiae*, shake flask, 30°C, 24 h	266 mg/L	[24]
		Glucose	*S. cerevisiae*, fed-batch, 30°C, 168 h	1.04 g/L	This study
		Glucose + L-Trp	*Zygosaccharomyces priorianus*, shake flask, 27°C, 46 h	585 mg/L	[21]

Molecular cloning

Plasmids and yeast strains were all constructed based on the yeast toolkit method [28], a modular, multipart plasmid constructing method based on the Golden Gate Assembly [29, 30]. In brief, (1) the PCR products, synthesized genes, and annealed oligos were used as the source DNAs to construct the part plasmids by *BsmBI* assembly. Point mutations to eliminate *BsaI* and/or *BsmBI* sites in the source DNAs were introduced into genes via overlap extension PCR [31]; (2) Cassette plasmids containing fully assembled transcriptional units that enable the expression of single genes were constructed by *BsaI* assembly of part plasmids; (3) Large plasmids containing multiple transcriptional units for expressing multiple genes were constructed by *BsmBI* assembly of the cassette plasmids [28]. For each step above, an assembly reaction mixture was prepared as follows: 0.5 µL of each source DNA or plasmid, 1 µL T4 DNA ligase buffer, 0.5 µL T7 DNA ligase, 0.5 µL *BsmBI* or *BsaI*. Water was added to the mixture to the final volume of 10 µL. Assemblies were conducted in a thermocycler with the following procedures: digestion and ligation (42 °C for 2 min, 16 °C for 5 min, 25 cycles), a final digestion (60 °C for 10 min), and heat inactivation (80 °C for 10 min).

The preparation of *E. coli* competent cells and *E. coli* transformation by the chemical method were similar to the protocols described by Chan et al. [32]. To make chemically competent cells, *E. coli* was grown in LB for ~ 2 h until OD_{600} reached 0.5. The obtained pellets were resuspended and washed twice in ice-cold 50 mM $CaCl_2$ solution and finally responded in the same solution to a final OD_{600} of ~ 12.5. For transformation, ~ 100 ng plasmid was mixed with 50 µL competent cells on ice for 30 min. The mixture-containing tube was heat-shocked in a 42 °C water bath for 45 s and then chilled on ice for 2 min. 1 ml LB medium was added and the cells were grown in a 37 °C shaker for 45 min. The outgrowth was then plated on LB plates containing the appropriate antibiotic.

Highly efficient yeast transformation with plasmids or linearized plasmids (by *NotI*) for genome integration was conducted using a method similar to the classical lithium acetate/ss carrier DNA/PEG method [33]. Briefly, to make competent cells, *S. cerevisiae* was grown in YPD at 30 °C, 220 rpm until OD_{600} reached ~ 0.5. Pellets were resuspended and washed twice with sterile diH_2O, once with 0.1 mM lithium acetate solution, and finally resuspended in 0.1 mM lithium acetate solution with a final OD_{600} of 5. For transformation, the pellet from 100 µL aliquot competent cells was obtained after centrifuging at 3,600 rpm for 5 min, then mixed with 240 µL of PEG4000 (50% w/v), 36 µL of lithium acetate (1.0 M), 25 µL of salmon testes ssDNA (2 mg/ml), 50 µL of diH_2O and plasmid DNA (100 ng). The mixture was incubated at 30 °C for 30 min, heat-shocked in a water bath at 42 °C for 30 min, and centrifuged at 3,600 rpm for 5 min. The pellets obtained were re-suspended in 200 µL of sterile diH2O and plated in auxotroph-selection agar plates. Clones grown after 3–4 day incubation at 30 °C were picked and verified by genome PCR and, subsequently, sequencing.

Genome editing

CRISPR-mediated homologous recombination was used to construct yeast strains with genomic modifications. The Cas9 in the CRISPR system introduces a double-strand break into the genome so as to select against the non-edited cells and hence improve the recombination

efficiency [34]. The guide RNAs (gRNAs) used in CRISPR for yeast gene deletion were designed using the online webserver (https://benchling.com/). The top 3 gRNA designs were chosen. Corresponding oligos were synthesized, annealed, and assembled into part plasmids, cassette plasmids, and finally into the multigene plasmids containing the Cas9 protein. To integrate gene(s) for overexpression from the genome, we constructed a second cassette/multigene plasmid by designing the transcription unit(s) to be integrated flanked by two arm sequences homologous to integrated sites. By contrast, a second plasmid for gene disruption was designed by introducing a sequence containing a premature stop codon (TAA) to the target gene flanked by two arm sequences homologous to integrated sites. The second plasmid was linearized by *NotI*, becoming the homologous repair DNA, and co-transformed with the CRISPR plasmid into the yeast strains. The intended genome modifications of the clones grown on agar plates were verified by genome PCR and, subsequently, sequencing. Curing the CRISPR plasmid was conducted by culturing the strains harboring the CRISPR plasmid in non-selective media for 24 h, plating on agar plates, and selecting clones that loosed selecting phenotypes.

Yeast fermentation in 24-well plates

Single clones (three biological replicates) were picked from the agar plates and inoculated into 24-well plates containing 2 ml YPD medium or SC media lacking the components to select for auxotrophic marker genes present on the plasmids. Cells were grown at 30 °C, 220 rpm for 24 h, and transferred into a fresh medium with an initial OD_{600} of 0.2. Cells were cultivated for 36 h unless otherwise specified. The optical density (OD_{600}) was measured by UV–Vis spectrophotometer 759 s (Shanghai Lengguang Technology Co. Ltd., Shanghai, China).

Fermentation in a 5 L bioreactor

The strain yBL542 with duplicates was used to produce IET under optimal conditions in a 5 L fed-batch bioreactor (Getinge Applikon, Delft, Netherlands). The seed cultures were grown in 2% YPD medium until OD_{600} reaches 8.0. Then, 50 ml of the seed cultures were transferred into the 5 L bioreactors containing 2 L 2% YPD medium. Fermentation was performed at 30 ℃. pH was maintained at 5.5 by the automated addition of 5 M NaOH. Airflow was set at 2.5 vvm (air volume/working volume/min), and the dissolved oxygen (dO_2) concentration was controlled above 40% saturation by agitation cascade (300–600 rpm). After the initial glucose was depleted, the stock solution (500 g/L) was fed periodically into the fermentation system to maintain glucose concentration under 5.0 g/L, which was monitored every 4 h by HPLC. The supplementary rate of glucose was ~ 3 g/ (L · h) (at 9.5–32 h) and adjusted to ~ 0.6 g/(L · h), which was maintained to the end of the fermentation. Yeast extract (500 g/L) was added into the bioreactor at 8, 16, 24, and 32 h with an equal volume of 125 ml. The whole fermentation process lasted for 168 h. The samples of fermentation cultures were taken every 12 h and stored at -20 ℃ until analysis. Glucose, ethanol, and IET contents were quantified from the supernatant part of the samples.

Quantification of metabolites

Extracellular metabolites from yeast fermentation were quantified by high-performance liquid chromatography (HPLC) equipped with a UV–Vis detector (SPD-20A/20AV) (Shimadzu, Kyoto, Japan). At the end of fermentation, 400 µL of the culture supernatant was mixed with an equal amount of anhydrous ethanol (100% v/v), mixed thoroughly, and centrifuged at 13,500 × g for 5 min. Next, 10 µL of a supernatant sample was injected into the system, and the aromatic compounds in the supernatant were separated by a Shimadzu Shim-pack GIST C18 column (4.6 mm × 150 mm, particle size 5 µm) (Shimadzu, Kyoto, Japan), using a method similar to the protocol described in the literature [35]. The column was kept at 30 °C. Samples were separated using a gradient with two solvents: (A) 20 mM potassium phosphate, pH 3.0, containing 1% acetonitrile; and (B) acetonitrile. The program started with linearly increased solvent B from 0 to 10% (0–6.0 min), then from 10 to 60% (6.0–25.0 min), then from 60 to 0% (25.0–26.0 min). Compounds related to AAAs metabolism were detected at the following elution times and wavelengths: L-Tyr (2.4 min, 215 nm), L-Phe (5.7 min, 215 nm), L-Trp (10.8 min, 215 nm), pPET (13.2 min, 215 nm), AA (15.5 min, 215 nm), IAA (18.5 min, 215 nm), PET (19.5 min, 215 nm), IET (20.2 min, 215 nm), PAA (24.3 min, 215 nm) (also see Fig. S1). Metabolite concentrations were quantified based on the calibration curves of purchased standards.

To quantify glucose and ethanol, filter the supernatant from 1 mL fermentation broth, and 10 µL of the sample was loaded into the HPLC system equipped with a refractive index detector (RID). Separation of glucose and ethanol was achieved using an Aminex HPX-87H column (300 mm × 7.8 mm, particle size 9 µm) (Bio-Rad Laboratories Inc., Hercules, USA). The column temperature was 40 °C, and the flow rate was 0.5 mL/min. 5‰ sulfuric acid was used as the solvent. Glucose was eluted at 11.0 min, and ethanol was eluted at 24.0 min.

Statistical analysis

All experiments in 24-well plates were repeated three times with biological replicates, with the data presented as mean ± standard derivation. Means were compared

using a two-tailed Student's *t* test [36]. The data was considered to be statistically significant when *P* values < 0.05. *P* values were represented as * $P<0.05$, ** $P<0.01$, *** $P<0.001$, and **** $P<0.0001$.

Results

System setup

Pathway analysis and engineering design

The entire pathway for IET de novo biosynthesis from glucose involves multiple steps. Based on the pathway structure, here we divided it into five sub-pathways (Fig. 1B): (1) glycolysis, which provides the precursor PEP for AAAs biosynthesis; (2) pentose phosphate pathway (PPP), which provides E4P, the second precursor for AAAs biosynthesis; (3) the shikimate pathway, which condenses PEP and E4P to CA; (4) the L-Trp pathway, which converts CA to L-Trp; and finally (5) the Ehrlich pathway that degrades L-Trp to IET. According to flux analysis, the metabolic flux through PEP is at least one order of magnitude greater than that through E4P in yeast [37]. As a result, we did not focus on increasing intracellular PEP in this study. Many studies showed that changes to a few gene targets increase intracellular E4P levels and hence balance the E4P/PEP ratio in yeast [35, 38], and we tested some of them, but interestingly, we did not obtain positive results (see discussion section). Thus, in this study, we were primarily interested in engineering the shikimate pathway (Sect. "Engineering the shikimate pathway (Module 1)"), the L-Trp pathway (Sect. "The L-Trp pathway (Module 2): the major bottleneck preventing flux into the L-Trp branch"), and the Ehrlich pathway (Sect. "Engineering the Ehrlich pathway (Module 4)") to improve IET production, which involves 15 reactions and the participation of more than 20 enzymes. Furthermore, the L-Phe/L-Tyr pathways compete with the L-Trp pathway for the common precursor CA (Fig. 1B), establishing the L-Phe/L-Tyr pathway as the competing pathway of IET biosynthesis. By *ARO7* deletion, we investigated the effect of blocking the flux into the L-Tyr/L-Phe pathways on IET production (Sect. "Roles of Aro7 (Module 3)").

Comparison of two S. cerevisiae strains for IET production

Two types of yeast strains (S288C derivatives and semi-industrial CEN.PK series) are commonly used in metabolic engineering research and synthetic biology due to a long history of comprehensive characterization and development of molecular biology tools for genetic manipulation. However, significant genomic differences between these two types of strains result in dramatically different physiology and metabolism [39]. Thus, prior to our systematic engineering of de novo IET production, we briefly compared the performance of two commonly used lab strains, S288C-derived BY4741 (*MATa, his3Δ1, leu2Δ0, met15Δ0, ura3Δ0*) [26] and CEN. PK-derived CEN.PK2-1D (*MATα ura3-52 leu2-3,112 trp1-289 his3-Δ1 MAL2-8c SUC2*) [27] for their performance of producing IET. The results show that BY4741 outperforms CEN.PK2-1D: after 48 h of cultivation in the SC medium, CEN.PK2-1D grew slightly better than BY4741, but BY4741 produced 68% more IET than CEN.PK2-1D (Fig. S2). As a result, in the following engineering work, we chose BY4741 as the parent strain.

Precursor-feeding experiments

We next conducted feeding experiments by adding 4-HPP (the precursor of pPET), PP (the precursor of PET), and L-Trp (the precursors of IET) into the cultures and measuring the production of fusel alcohols (Fig. S3). The conversion rates of these precursors to fusel alcohols were relatively low (< 20% at 96 h). However, the amount of each fusel alcohol produced correlated positively with its precursor concentrations (Fig. S3). Thus, in the following study, we used pPET, PET, and IET titers as surrogates for metabolic fluxes toward L-Tyr, L-Phe, and L-Trp branches, respectively. Despite the fact that in this study, IET is our target compound and pPET and PET are by-products from the competing L-Tyr/L-Phe branches, pPET and PET are actually also important compounds that were produced in engineered *E. coli* and yeast [40–47].

Engineering the shikimate pathway (Module 1)

We then began our metabolic engineering efforts in order to divert more flux from the central metabolic pathway into AAAs biosynthesis (Fig. 1B). The shikimate pathway converts PEP and E4P into CA through seven reactions, the first of which is catalyzed by the DAHP synthase isozymes Aro3 and Aro4. Aro1, a pentafunctional enzyme, catalyzes the following five reactions. Finally, the shikimate pathway is completed by the chorismate synthase Aro2. L-Phe and L-Tyr allosterically inhibit Aro3 and Aro4, respectively, at the enzyme activity level. Numerous studies have confirmed that the first step catalyzed by Aro3/Aro4 is a major checkpoint controlling the flux into AAAs biosynthesis and overexpression of the feedback-insensitive mutants $ARO3^{K222L}$ and/or $ARO4^{K229L}$ (or $ARO4^{Q166K}$, or $ARO4^{G226S}$) usually results in efficient condensation of E4P and PEP. [35, 48–50]

Inspired by the information mentioned above, we overexpressed additional copies of the feedback-insensitive $ARO4^{K229L}$ under the control of the strong institutive promoter pTDH3, without knocking out the endogenous wild-type *ARO4* (Fig. 2B, 2). Opening this valve significantly raised the titers of all three fusel alcohols. We investigated the effects of different expression levels by

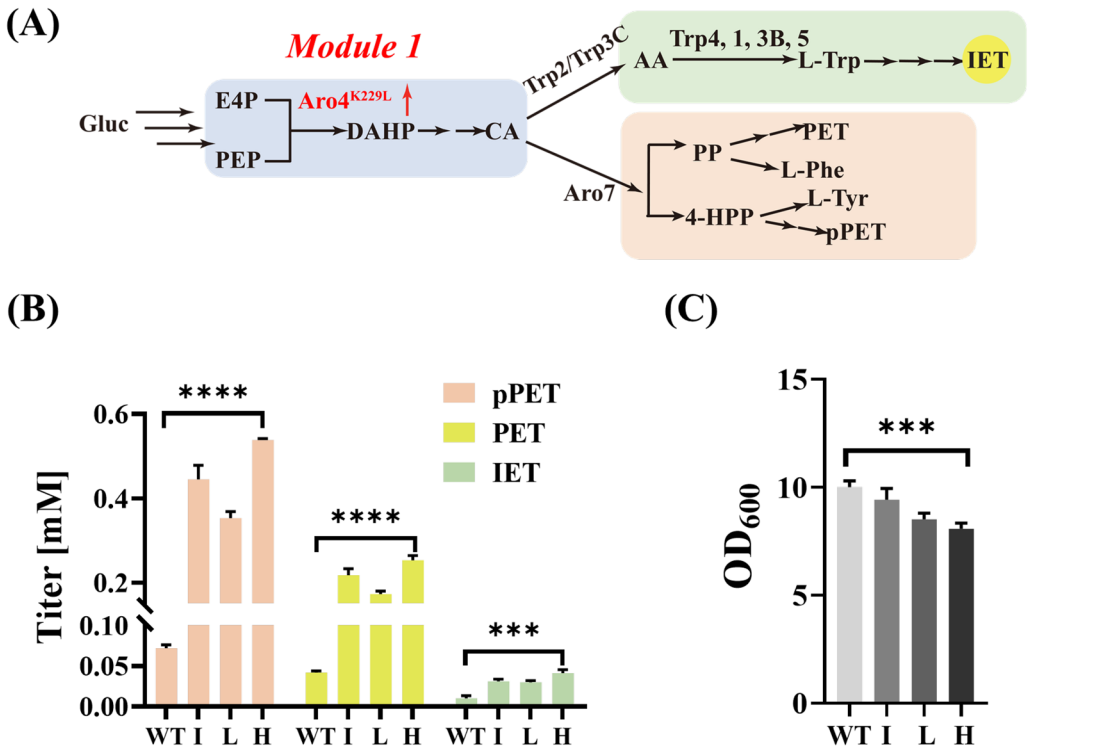

Fig. 2 Engineering Module 1 by overexpressing the feedback-insensitive *ARO4*^{K229L} in BY4741. **A** Schematic diagram of the AAAs pathway, implying the *ARO4*^{K229L} is upregulated. **B** Titers of pPET, PET, and IET after 36 h cultivation in SC medium. **C** Cell densities (OD_{600}) after cultivation in an SC medium for 36 h. WT, wild-type BY4741; I, BY4741 containing genomically integrated pTDH3–ARO4^{K229L}–tENO1 cassette at *ura3* locus; L, BY4741 with pTDH3–ARO4^{K229L}–tENO1 cassette placed on a low-copy plasmid with; H, BY4741 with pTDH3–ARO4^{K229L}–tENO1 cassette placed on a high-copy plasmid

inserting the *ARO4*^{K229L} expressing cassette into the chromosome (single-copied) or placing it on a CEN6/ARS4-based low-copy plasmid or a 2μ-based high-copy plasmid. After 36 h of fermentation in SC medium, overexpressing *ARO4*^{K229L} from high-copy plasmid resulted in the greatest improvement in titers (7.5-fold for pPET, 6.0-fold for PET, and 4.1-fold for IET, respectively), compared with wild-type BY4741 (0.01 ± 0.003 mM) (Fig. 2B). We do, however, noticed an increase in growth burden due to increased *ARO4*^{K229L} copies. Putting *ARO4*^{K229L} in a high-copy plasmid reduced cell density by 20% compared to BY4741 (Fig. 2C).

The L-Trp pathway (Module 2): the major bottleneck preventing flux into the L-Trp branch

In *S. cerevisiae*, L-Trp is synthesized from CA through five reactions, catalyzed by Trp2 (anthranilate synthase)/Trp3C (N-terminal glutamine amidotransferase domain of Trp3), Trp4 (anthranilate phosphoribosyl transferase), Trp1 (phosphoribosylanthranilate isomerase), Trp3B (C-terminal indole-3-glycerol-phosphate synthase domain of Trp3) and Trp5 (bifunctional L-Trp synthase) (Fig. 1B). The activity of Trp2 is feedback inhibited by L-Trp [51]. In an earlier study, *TRP1-5* (*TRP2*^{fbr}) was overexpressed under the control of native promoters and from a high-copy plasmid, resulting in a tenfold increase in L-Trp flux compared to the wild-type strain when the precursor AA was supplemented [52]. In two recent studies, the feedback-insensitive *TRP2*$^{S65R,\ S76L}$ were overexpressed in *S. cerevisiae*, resulting in increased productions of L-Trp [53] and L-Trp-derived psilocybin [54]. However, in general, the L-Trp pathway in yeast has received less attention. As a result, we comprehensively described it in this study.

We first tested the effect of overexpressing *TRP2*$^{S65R,\ S76L}$ in yeast strain yBL502, which has one genome-integrated *ARO4*^{K229L} at the *ura3* locus and native wild-type *TRP1-5*. Overexpression of *TRP2*$^{S65R,\ S76L}$ resulted in an increase in IET titer over the parent strain (Fig. 3B). When *TRP2*$^{S65R,\ S76L}$ was placed under the control of the constitutive pHHF2 promoter and from a low-copy plasmid, the highest titer (3.8-fold improvement) was obtained. In this case, the pPET level was slightly lower (8%), while the PET level was slightly higher (18%). (Fig. 3B).

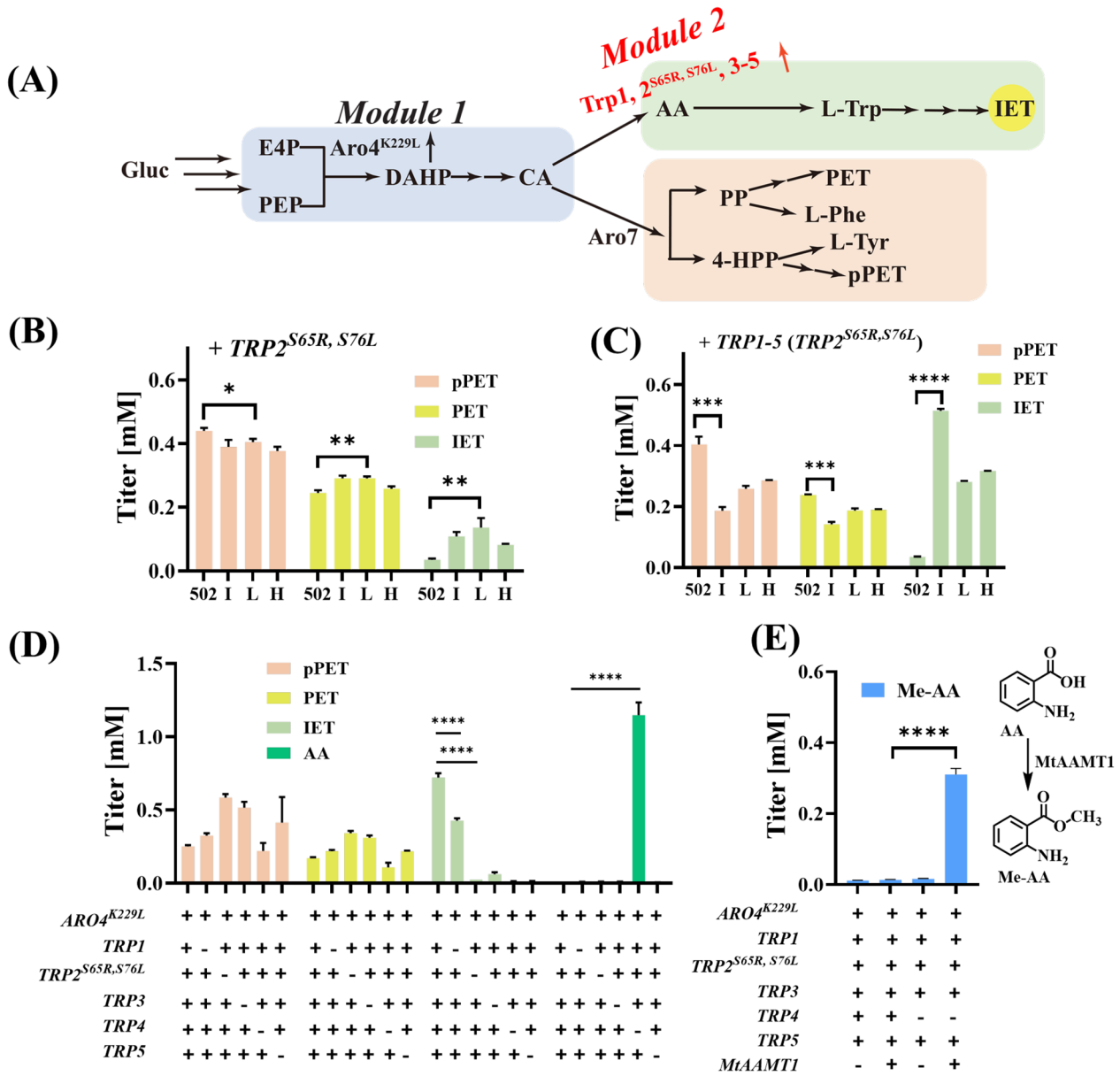

Fig. 3 Engineering the L-Trp synthesis (Module 2) for improved IET production. **A** Schematic diagram of the AAAs pathway indicating that the up-regulation of the entire L-Trp pathway was investigated. **B** Effects of upregulating feedback-insensitive *TRP2*$^{S65R, S76L}$ on the production of fusel alcohols. In the parent strain that overexpresses *ARO4*^{K229L} (yBL502), upregulating *TRP2*$^{S65R, S76L}$ was achieved by overexpressing *TRP2*$^{S65R, S76L}$ from the chromosome (I), low-copy plasmid (L), or high-copy plasmid (H). **C** Effects of upregulating the entire L-Trp pathway genes (*TRP1*, *TRP2*$^{S65R, S76L}$, and *TRP3-5*) on the production of fusel alcohols. In the parent strain that overexpresses *ARO4*^{K229L} (yBL502), upregulating was achieved by overexpressing the entire L-Trp pathway genes from the chromosome (I), low-copy plasmid (L), or high-copy plasmid (H). **D** Top-down approach to identify the bottleneck steps that restrict metabolic flux into the L-Trp branch. **E** Synthesis of Me-AA by expressing *MtAAMT1* in the AA accumulating strain. All samples above taken for metabolite quantification were taken after 36 h cultivation of yeast strains in the SC medium

Next, we overexpressed additional copies of *TRP1-5* (*TRP2*$^{S65R, S76L}$) in yBL502, with each gene controlled by a strong constitutive promoter, which surprisingly increased IET titer by up to 15-fold (Fig. 3C). When *TRP1-5* (*TRP2*$^{S65R, S76L}$) was integrated into the genome, the strain yBL518 achieved the greatest increase. Furthermore, an increase in IET titer was associated with a drop in pPET and PET titers of up to 54% and 41%, respectively, implying that more flux was diverted from the L-Tyr/L-Phe branches into the L-Trp branch. Such findings also point to additional rate-determining steps among the reactions catalyzed by Trp1, 3, 4, and/or 5.

We then used a top-down approach to identify such bottleneck step(s) by removing each of the five additional overexpressed genes (*TRP1*, $TRP2^{S65R,\ S76L}$, *TRP3*, *TRP4*, *TRP5*) (Fig. 3D), from which we gained many insights into AAAs metabolism of yeast:

(1) Removing the overexpressed *TRP1* led to 40% reduced IET titer while removing overexpressed $TRP2^{S65R,\ S76L}$, *TRP3*, *TRP4*, or *TRP5* resulted in at least 92% reduced IET titers (Fig. 3D), implying overexpressing all five genes are necessary for efficiently diverting more flux into the L-Trp branch.

(2) Removing the overexpressed *TRP4* almost eliminated IET production without increasing by-product titers (pPET and PET) (Fig. 3D), implying the accumulation of some other metabolite(s). Indeed, by examining the HPLC profiles, we determined that the accumulated metabolite is AA (Fig. 3E), the substrate of Trp4. Thus, by overexpressing $ARO4^{K229L}$, *TRP1*, $TRP2^{S65R,\ S76L}$, *TRP3*, and *TRP5*, we obtained an AA accumulating and L-Trp prototypic strain yBL522, which would be more valuable than the previously reported AA overproducing but L-Trp auxotrophic strain [55]. As AA and its derivatives are building blocks of many valuable natural products [56], our AA overproducing strain yBL522 could serve as an excellent heterologous host for natural product synthesis. As a proof-of-concept, we introduced yBL522 with the gene *MtAMTA1* from *Medicago truncatula* [55, 57], encoding an anthranilic acid methyltransferase. This enzyme converts AA to methyl anthranilate (Me-AA), a compound of grape scent and flavor with wide industrial applications. Indeed, after 36 h of cultivation in SC medium, the resulting strain yBL551 produced 0.31 ± 0.01 mM Me-AA, which is 23-fold more than the strain yBL552 that overexpresses *TRP1-5* ($TRP2^{S65R,\ S76L}$) (Fig. 3E).

(3) We saw significantly higher pPET and/or PET when removing overexpressed $TRP2^{S65R,\ S76L}$, or *TRP3* (Fig. 3D), highlighting Trp2 and Trp3's critical roles in controlling the flux toward L-Trp branches or L-Tyr/L-Phe branches, because Trp2/Trp3C catalyzes the first reaction of the L-Trp branch (Fig. 1B).

(4) When overexpressed *TRP5* was removed, IET production was also abolished but pPET and PET titers were not improved (Fig. 3D). We suspected I3GP accumulation in this strain, because Trp5 catalyzes the final step in the L-Trp branch that converts I3GP to L-Trp (Fig. 1B). However, because we cannot quantify I3GP at the moment, this hypothesis needs to be verified.

Finally, because genome integration resulted in the highest IET titer (0.51 ± 0.01 mM) when compared with that expressed from both low-copy and high-copy plasmids (Fig. 3C), and because genomic integration has several advantages, including genetic stability and low cell burden, we only constructed and used plasmid-free (genomically integrated) strains for IET production in the rest of the study.

Roles of Aro7 (module 3)

After 36 h cultivation in SC medium, 0.25 mM pPET, 0.17 mM PET, and 0.72 mM IET were produced by the strain yBL518 that additionally overexpresses $ARO4^{K229L}$, *TRP1-5* ($TRP2^{S65R,\ S76L}$) from genome besides the endogenous *ARO4* and *TRP1-5* (Fig. 3D). The fact that this strain continued to produce a significant amount of pPET and PET motivated us to investigate whether more work can be done to divert more flux from the L-Tyr/L-Phe branches into the L-Trp branch for increased IET production. At the node CA, the flux from the upstream shikimate pathway splits: (1) into the L-Tyr/L-Phe branches via the chorismate mutase Aro7; and (2) into the L-Trp branch via Trp2/Trp3C, which converts CA to AA. The disruption of *ARO7* could theoretically completely block the flux into the L-Tyr/L-Phe branches. Indeed, *aro7Δ* lowered pPET and PET for both yBL502, which only overexpressed $ARO4^{K229L}$, and yBL518, which overexpressed $ARO4^{K229L}$ and *TRP1-5* ($TRP2^{S65R,\ S76L}$) (Fig. 4B). The residual pPET and PET produced by the two strains were most likely formed from L-Tyr and L-Phe contained in the SC medium (initial concentrations: 0.42 mM for L-Tyr and 0.46 mM for L-Phe, respectively). The introduction of *aro7Δ* to yBL502 also resulted in increased IET and L-Trp (Fig. 4B). However, for yBL518, the introduction of *aro7Δ* resulted in a 5% decrease in IET and a twofold increase in L-Trp (Fig. 4B). The unexpected accumulation of L-Trp up to 0.24 mM by *aro7Δ* suggests that there is another bottleneck step(s) in the downstream Ehrlich pathway. Intermediate (s) and/or end product(s) exist in L-Tyr/L-Phe branches that are required to convert L-Trp to IET. We then examined the pathway and discovered that transaminase Aro9 uses PP as a substrate for accepting amino groups from L-Trp [19]. We then fed PP or 4-HPP into the SC medium to cultivate yBL517 (yBL518 with *aro7Δ*) (Fig. S4). Indeed, adding PP to the medium improved the conversion of L-Trp to IET slightly, but it was still less effective than using the strain yBL518. Feeding 4-HPP, on the other hand, was ineffective (Fig. S4).

Engineering the Ehrlich pathway (module 4)

In yeast, the Ehrlich pathway catabolizes aliphatic (L-Leu, L-Val, L-Ile), sulfur-containing (L-Met), and aromatic

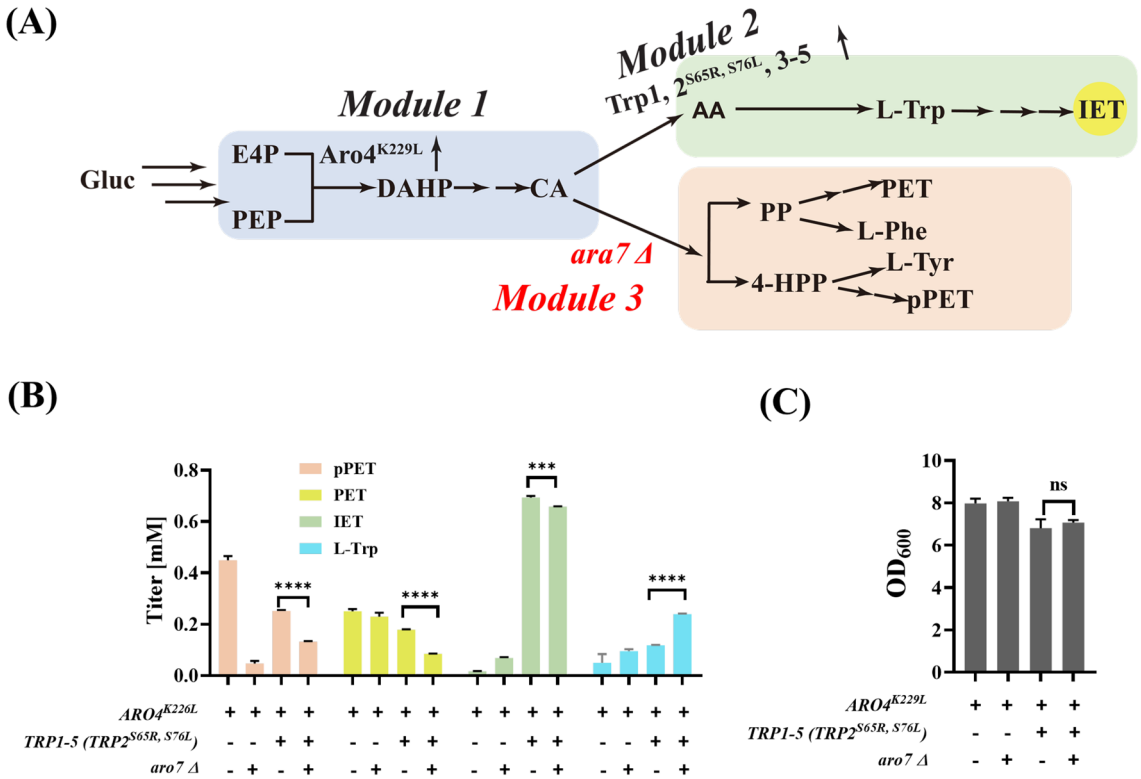

Fig. 4 Effects of *aro7Δ* (engineering Module 3) on the production of L-Trp and IET after cultivation in SC media for 36 h. **A** Schematic diagram of the AAAs pathway. **B** Effects of *aro7Δ* on the production of fusel alcohols and L-Trp. Two parent strains tested were yBL502 that overexpresses $ARO4^{K226L}$ and yBL518 that overexpresses $ARO4^{K226L}$, *TRP1*, $TRP2^{S65R, S76L}$, and *TRP3-5*. **C** OD_{600}

(L-Tyr, L-Phe, L-Trp) amino acids, resulting in the formation of aliphatic and aromatic fusel alcohols or fusel acids [25]. Reversible transamination of amino acids, decarboxylation of α-keto acids, and reduction/oxidation of fusel aldehyde to fusel alcohols/acids are the three steps in the Ehrlich pathway [25] (Fig. 1B). Each step is catalyzed by more than one isozyme with various substrate specificities. For example, the two transaminases Aro8 and Aro9 have broad substrate specificity but primarily function as AAA aminotransferases, preferentially using 2-OG and phenylpyruvate as amino acceptors, respectively [58]. The irreversible decarboxylation step commits α-keto acids to the Ehrlich pathway, which requires the cofactor thiamine pyrophosphate (TPP). This reaction could be catalyzed by four α-keto acid decarboxylases (Aro10, Pdc1, Pdc5, and Pdc6). Thi3 has a similar sequence to the preceding four but lacks decarboxylase activity, preferring to play a regulatory role in thiamine biosynthesis [59]. The reduction or oxidation of fusel aldehydes is the final step. The cultivation conditions determine whether reduction or oxidation occurs. Similar to the conditions in this study (glucose-grown), amino acids are almost entirely converted to fusel alcohols by ethanol dehydrogenases (Adh1-5) or Sfa1 (a formaldehyde dehydrogenase) [22, 25]. In contrast, aldehyde dehydrogenases Ald1-6 catalyze the conversion of amino acids to fusel acids in aerobic glucose-limited chemostat cultures with various amino acids as nitrogen sources [25].

The accumulation of L-Trp in the strain yBL517 suggests that there is a bottleneck step(s) in the Ehrlich pathway that prevents efficient L-Trp to IET conversion (Fig. 4B). Given that multiple isozymes catalyze each step of the Ehrlich pathway, we decided to take a bottom-up approach to debottleneck the rate-determining step(s) and hence improve IET production even further.

(1) First, we overexpressed another copy of *ARO8* or *ARO9* from the genome using a constitutive promoter (Fig. 5B, C). Overexpression of either gene resulted in a more efficient conversion of L-Trp to IET in the SC medium. The effect of overexpressing *ARO9* was more visible: after 36 h of fermentation, the strain yBL533 (yBL517 with overexpressed *ARO9*) had 25% higher IET (0.72 ± 0.02 mM) and 80% lower extracellular L-Trp (Fig. 5B). We wondered if cultivating yBL533 in the YPD medium would result in further improved IET titer, since based on our experience, this rich medium sup-

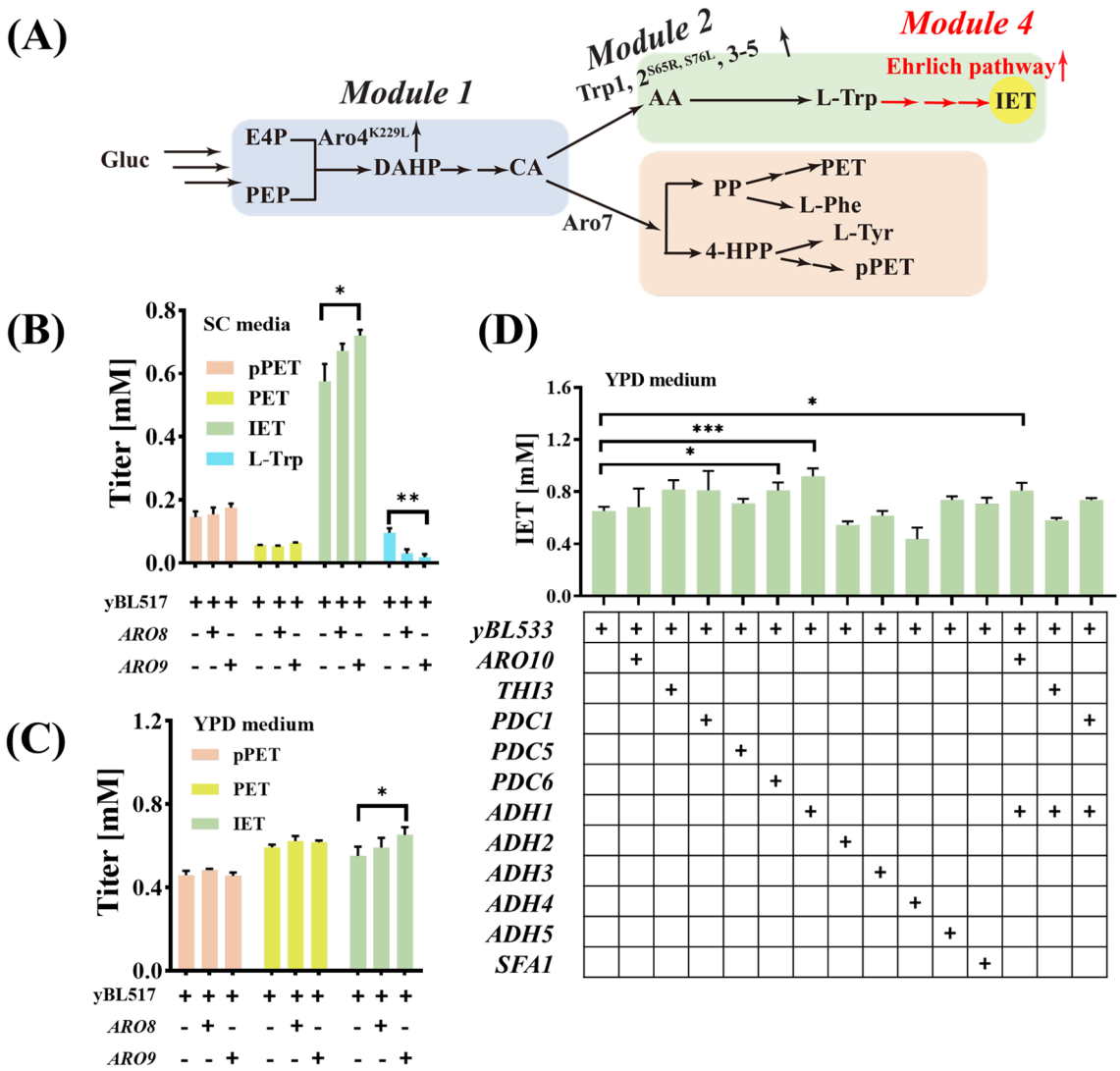

Fig. 5 Engineering the Ehrlich pathway (Module 4) for improved IET production. **A** Schematic diagram of the AAAs pathway indicates the Ehrlich pathway's up-regulation is investigated. The effects of upregulating the first step of the Ehrlich pathway (transamination) on the production of fusel alcohols were evaluated upon 36 h cultivation in SC media **B** and YPD medium (**C**). The parent strain used is yBL517 that overexpresses *ARO4*^{K229L}, *TRP1*, *TRP2*$^{S65R, S76L}$, *TRP3-5*, and has *aro7Δ*). **D** Effects of upregulating the second and third steps of the Ehrlich pathway on the production of fusel alcohols are tested in the YPD medium. The parent strain used is yBL533 that overexpresses *ARO4*^{K229L}, *TRP1*, *TRP2*$^{S65R, S76L}$, *TRP3-5*, *ARO9*, and has *aro7Δ*

ports better yeast growth than SC medium. Indeed, the ODs of all strains tested were doubled when grown in YPD (Fig. S5A). We also discovered that pPET and PET for all strains were significantly increased, reaching ~ 0.45 mM and ~ 0.6 mM, respectively (Fig. 5C). However, when compared to the SC medium, the accumulated IET was nearly unchanged (Fig. 5B).

(2) We suspected that the failure to improve IET further when cultivation was transferred from SC medium to YPD medium is due to insufficient gene expression (enzyme dosage) in the remaining two steps of the Ehrlich pathway. We tested this hypothesis in yBL533 by overexpressing genes encoding enzymes from the remaining two steps of the Ehrlich pathway (Figs. 5D, S5B, and S5C). The effect of single-gene overexpression on IET production was positive (such as for *PDC6* and *ADH1*), neutral (such as for *PDC5*, *ADH5*, and *SFA1*), or negative (such as for *ADH2*, *ADH3*, and *ADH4*). We then tested a few combinations of the overexpressed genes in the last two steps at the

background of yBL533; however, none of them showed beneficial effects as compared with single-gene expressions (Fig. 5D). We measured the final OD_{600} (Fig. S5B) and hence calculated the normalized production (IET titer/OD_{600}) (Fig. S5C). The best strain that overexpresses *ADH1* (yBL542), produced 0.92 ± 0.06 mM 40% more IET than yBL533 in the YPD medium. This increase in titer was due to increased biomass rather than increased Ehrlich pathway flux toward IET, as OD_{600} increased by 64% (Fig. S5B) while the normalized production decreased by 14% (Fig. S5C). Overexpression of Ehrlich pathway genes had an apparent effect on final cell density: OD_{600} varies between -32% and 64% compared to the parent strain yBL533 (Fig. S5B). In contrast, the change in IET production caused by overexpression of the Ehrlich pathway genes was minor (Fig. S5C), implying the limited effects of changing the flux toward IET. The only exception is *ARO10* overexpression, which resulted in a 54% increase in normalized production. It does, however, cause a 32% decrease in OD_{600}, so its effect on titer was negligible.

The above findings are most likely related to the nature and overall metabolic and physiological effects of the Ehrlich pathway, which is a three-step pathway catalyzed by multiple isozymes that converts seven hydrophobic amino acids to the corresponding fusel alcohols/acids [25]. The last two steps are also used in converting pyruvate to ethanol in glycolysis. The Ehrlich pathway thus has the roles of not only amino acid degradation but also NAD^+ regeneration [60] and even in quorum sensing [25]. Overexpression of specific isozymes in the Ehrlich pathway thus has complex effects on metabolism, biomass, and, ultimately, IET titer.

Optimized IET production by fed-batch fermentation

Finally, in a 5 L fed-batch bioreactor, we used the best-engineered strain yBL542, which overexpressed *ARO4*^{K229L}, *TRP1-5* (*TRP2*$^{S65R, S76L}$), *ARO9*, and *ADH1*, as well as has *aro7Δ*, to produce IET (Fig. 6A, B). We first cultured yBL542 in a YDP medium and adjusted the glucose feeding rate to keep its concentration between 0.5 and 5 g/L after the initial depletion (Fig. 6A). Both cell density and IET titer were rapidly boosted under this condition, reaching plateaus at 72 h (OD_{600} = 47 and IET titer = 3.4 mM). However, we saw gradually accumulated ethanol up to 5.8% in the culture, implying that the strain is performing sub-optimally in the bioreactor. Therefore, we optimized the fermentation conditions by supplementing yeast extract (125 ml, 500 g/L) at 8, 16, 24, and 32 h time points, similar to the study of producing tyrosol and salidroside using engineered *S. cerevisiae* [43]. The accumulated ethanol peaked at 32 h this time and then gradually decreased. The cell density reached higher plateaus at 120 h (OD_{600} = 47), and the IET titer steadily increased until reaching 6.5 mM (= 1.04 g/L) at the end of 168 h fermentation, the highest titer reported thus far. To calculate the theoretical maximum yield of IET, we conducted flux balance analysis (FBA) of the *S. cerevisiae* genome-scale metabolic model Yeast8 [61], using the COBRA toolbox [62]. Without any restriction, the theoretical maximum yield of glucose to IET is 0.38 g/g. Thus, the IET produced through fed-batch fermentation in this study represented 13.2% of the theoretical maximum yield of such an ideal condition.

Discussion

The biosynthesis pathway for AAAs (L-Tyr, L-Phe, and L-Trp) is ubiquitous in all microorganisms. The AAAs pathway, along with its downstream branches, represents one of the most valuable biosynthetic pathways, from which a myriad of valuable commodity chemicals, specialty chemicals, and valuable natural products [19, 63–65]. The model prokaryote *E. coli* and the model eukaryote *S. cerevisiae* have been most commonly used to heterologously produce AAA-derived valuable chemicals, owing to advantages such as fast growth, well-known genetic background, and readily available tools for genetic modifications. In the majority of reported cases, AAA-derived products were typically produced more efficiently in *E. coli* (g/L scale) than in *S. cerevisiae* (mg/L scale), and some have been commercialized [65]. *S. cerevisiae*, on the other hand, can express membrane-associated eukaryotic enzymes [66, 67]. As a result, it attracts special attention as the preferred host for synthesizing valuable natural products from fungi and plants [68–70].

Most successful metabolic engineering studies in *S. cerevisiae* used intermediates from the shikimate pathway and the L-Tyr/L-Phe branches [65]. Heterologous pathways were introduced into chassis yeast strains with increased flux in the shikimate pathway and L-Tyr branch or L-Phe branch to synthesize a wide range of non-native chemicals, including industrially important precursors, such as muconic acid [71] and p-coumaric acid [35], analgesic opioids [72], health-promoting hydroxytyrosol [73], and many more. Two recent reviews summarized a nearly complete list of these valuable chemicals produced by yeasts [63, 65].

On the other hand, the biosynthesis of L-Trp-derived compounds in engineered *S. cerevisiae* has less be explored; examples reported in recent years include the production of plant-derived anti-cancer drugs and their precursors [74, 75], L-Trp itself [53], the sleep hormone melatonin and its precursor 5-hydroxytryptophan [76,

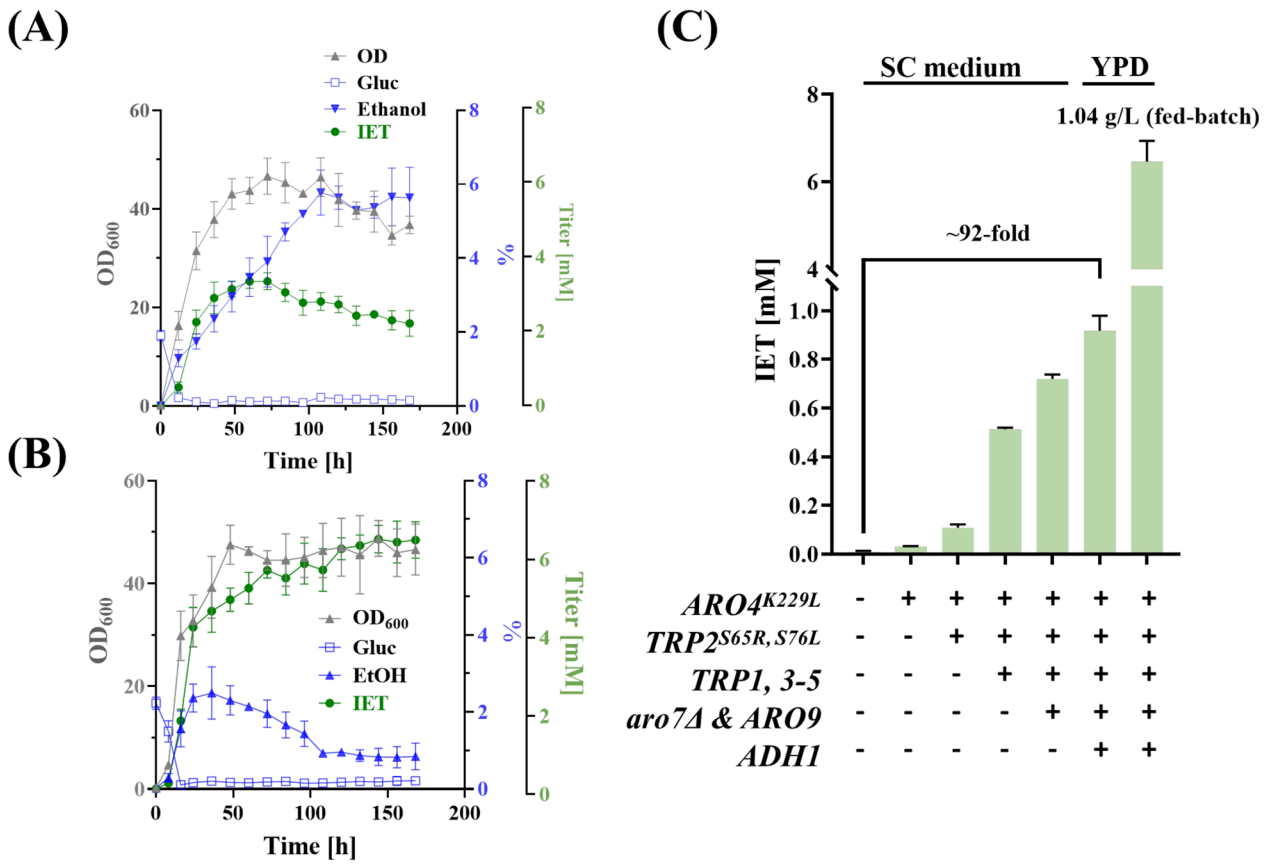

Fig. 6 Fed-batch fermentation for optimized IET production and summarized achievements in this study of engineering *S. cerevisiae* for improved IET production. IET was produced by the engineered strain yBL542 in a 5 L fed-batch bioreactor, using YPD medium with supplemented glucose to maintain its concentration between 0.5 and 5 g/L (**A**) and additionally supplemented yeast extract at 8, 16, 24, and 32 h (**B**). **C** Summary of IET production by the yeast strains constructed in this study

77], and the psychedelic prodrug psilocybin [54], and halogenated tryptophan and tryptamine derivatives [78]. Common features in these proof-of-concept studies are the low product titers/yields, which, based on this study, could probably be attributed to the low flux toward the L-Trp branch.

In this study, using the synthesis of IET (another L-Trp-derived valuable chemical) [1] as an example, we systematically characterized and optimized the L-Trp metabolic pathway in *S. cerevisiae*. (1) We again confirmed that the first step in the shikimate pathway catalyzed by Aro3/Aro4 isozymes is a primary checking point for the entire AAA metabolism and overexpressing the well-known feedback-insensitive $ARO4^{K229L}$ can dramatically diverse a large amount of flux from central metabolism into AAA metabolic branch (Fig. 2); (2) We identified the five-step L-Trp pathway is the major bottleneck. Increasing flux into the L-Trp branch requires simultaneous overexpression of wild-type *TRP1*, *TRP3*, *TRP4*, *TRP5*, and the feedback-insensitive $TRP2^{S65R,\ S76L}$ (Fig. 3). (3) Owing to the global roles of the Ehrlich pathway in regulating metabolism and physiology [25], upregulating relevant enzymes has complex effects on the conversion of L-Trp to IET. For example, the most effective manipulation that improved IET titer came from overexpressing *ADH1*, which, interestingly, was caused by improved cell growth rather than enhancing the flux (Figs. 5 and S5). We finally obtained an engineered strain that produces IET 0.92 mM (148.3 mg/L) in a 24-well plate and 6.46 mM (1.04 g/L) by fed-batch fermentation, representing 92-fold and ~ 650-fold improvements over the starting strain BY4741, respectively (Fig. 6C). This also represents the first report of gram-level IET production by using microbial production approaches, holding potential for it to be developed as a green/sustainable alternative over the traditional synthetic approach for IET production. IET titers of representing yeast strains engineered in this study are listed in Table 2.

Besides, studies indicate at the entrance of AAAs metabolism, the flux through PEP is at least one order of

Table 2 Summary of the IET produced by representing strains engineered in this study

Strain name	Genotype	IET Titer [mM] (Fold)	Culture condition
BY4741	WT	0.01 ± 0.003 (1)	2ml 24-well plate, SC
yBL502	*ARO4*^{K229L} ↑	0.03 ± 0.003 (3)	2ml 24-well plate, SC
yBL514	*ARO4*^{K229L} ↑ *TRP2*$^{S65R, S76L}$↑	0.11 ± 0.01 (11)	2ml 24-well plate, SC
yBL518	*ARO4*^{K229L}↑ *TRP1-5* (*TRP2*$^{S65R, S76L}$) ↑	0.51 ± 0.01 (51)	2ml 24-well plate, SC
yBL533	*ARO4*^{K229L} ↑ *TRP1-5* (*TRP2*$^{S65R, S76L}$) ↑ *aro7Δ* *ARO9* ↑	0.72 ± 0.02 (72) 0.65 ± 0.04 (65)	2ml 24-well plate, SC 2ml 24-well plate, YPD
yBL542	*ARO4*^{K229L} ↑ *TRP1-5* (*TRP2*$^{S65R, S76L}$) ↑ *aro7Δ* *ARO9* ↑ *ADH1* ↑	0.92 ± 0.06 (92) 3.37 ± 0.16 (340) 6.46 ± 0.34 (646)	2ml 24-well plate, YPD 5L fermenter, batch, YPD 5L fermenter, fed-batch, YPD

magnitude greater than that through E4P in yeast [37]. Thus, genetic modifications that increase the availability of E4P were demonstrated effective in improving the production of chemicals derived from AAAs metabolism [35, 38, 39, 65, 71, 79–81]. We tested most of these genetic changes (Fig. S6). However, none of them showed positive effects on improving IET production, which could be attributed to the difference in strain background (BY4741 in this study vs. other yeast strains in those studies) and the epistatic effects of the already-introduced genetic modifications in yBL518.

Finally, in this study, we mainly engineered the expression level of pathway genes/enzymes that are directly related to yeast L-Trp metabolism for enhanced IET production. However, it should be noted that many cofactors (such as NADH/NAD$^+$, NADPH/NADP$^+$, pyridoxal 5'-phosphate, and thiamine pyrophosphate), as well as metabolites not listed as the "nodes" in the pathways (such as L-glutamine, L-serine, 2-oxoglutarate, etc.), also participate in the reactions of AAAs metabolism. They would cause a major limitation to the pathways. Thus, systems biology approaches, such as genome-scale-model-guided prediction [82] and high-throughput screening/selection [34], could help identify more gene targets with modifications that divert more metabolic flux toward the L-Trp branch for enhanced production of IET or other value-added chemicals.

Conclusions

In this study, we systematically characterized *S. cerevisiae*'s AAAs metabolism, with a particular emphasis on the less-studied L-Trp branch for synthesizing the L-Trp-derived natural product IET. We used the modular engineering strategy to comprehensively engineer the shikimate pathway, the L-tryptophan pathway, the competing L-Tyr/L-Phe branches, and the Ehrlich pathway, resulting in a yeast mutant capable of producing IET up to 1.04 g/L via fed-batch fermentation. More importantly, our engineering process revealed many insights into AAAs metabolism and regulation of *S. cerevisiae*. We also discovered yeast mutants that accumulate AA and L-Trp during our engineering process. They could be further developed into the heterologous chassis to synthesize a variety of valuable secondary metabolites derived from fungi and plants.

Abbreviations

Metabolites

AA	Anthranilic acid
CPdRibp	1-(2-Carboxyphenylamino)-1-deoxy-D-ribulose 5-phosphate
CA	Chorismate
DAHP	3-Deoxy-D-arabinoheptulosonate-7-phosphate
EPSP	5-Enolpyruvylshikimate-3-phosphate
E4P	Erythrose 4-phosphate
F1,6BP	Fructose 1,6-bisphosphate
F6P	Fructose 6-phosphate
Glc	Glucose
G6P	Glucose 6-phosphate
G3P	Glyceraldehyde 3-phosphate
4-HPP	4-Hydroxyphenylpyruvate
IAA	Indole-3-acetate
IAC	Indole-3-acetaldehyde
IET	Tryptophol (indole-ethanol)
I3GP	Indole-3-glycerol phosphate
IPY	Indole-3-pyruvate
PAA	4-Hydroxyphenyl acetate
L-Phe	L-phenylalanine
PET	Phenylethanol
PP	Phenylpyruvate
PEP	Phosphoenolpyruvate
pPET	4-Hydroxyphenylethanol
N-PRAA	N-(5-phospho-β-D-ribosyl)anthranilate
PRE	Prephenate
Ru5P	Ribulose 5-phosphate
L-Trp	L-tryptophan
L-Tyr	L-tyrosine
X5P	Xylulose 5-phosphate

Enzymes

Adh1/2/3/4/5/Sfa1	Alcohol dehydrogenases
Aro1	Pentafunctional protein
Aro2	Chorismate synthase
Aro3/Aro4	DAHP synthase isozymes
Aro7	Chorismate mutase
Aro8/Aro9	Aromatic amino acid transaminases
Aro10/Thi3/Pdc1/5/6	Decarboxylases
Pha2	Prephenate dehydratase
Tal1	Transaldolase
Tkl1	Transketolase
Trp1	Phosphoribosylanthranilate isomerase
Trp2/Trp3C	Anthranilate synthase
Trp3B	InGP synthase
Trp4	Anthranilate phosphoribosyl transferase
Trp5	Bi-functional L-Trp synthase
Tyr1	Prephenate dehydrogenase
Zwf1	Glucose 6-phosphate dehydrogenase

Supplementary Information

The online version contains supplementary material available at https://doi.org/10.1186/s13068-024-02576-4.

Supplementary material 1.

Author contributions

Ye Li: conceptualization, methodology, formal analysis, writing—original draft, writing—review and editing, supervision, funding acquisition; Jingzhen Sun: validation, methodology, investigation, writing—original draft; Zhenhao Fu: investigation; Yubing He: investigation; Xiaorui Chen: investigation; Shijie Wang: investigation; Lele Zhang: investigation; Jiansheng Jian: investigation; Weihua Yang: project administration; Chunli Liu: project administration; Xiuxia Liu: project administration; Yankun Yang: project administration; Zhonghu Bai: resources, funding acquisition.

Funding

This work was supported by the Key Laboratory of Industrial Biotechnology of the Ministry of Education (Grant No. KLIB-KF202201 to Y. L.) and the National Natural Science Foundation of China (Grant No. 21878124 to Z. B.)

Availability of data and materials

The authors declared that the data supporting the findings of this study are available within the article and its Supplementary material file. The datasets generated and analyzed during this study are available from the corresponding authors upon request.

Declarations

Competing interests

The authors declared no conflict of interest regarding the publication of this work.

Received: 4 May 2024 Accepted: 5 October 2024
Published online: 16 October 2024

References

1. Palmieri A, Petrini M. Tryptophol and derivatives: Natural occurrence and applications to the synthesis of bioactive compounds. Nat Prod Rep. 2019;36:490–530.
2. Sarwar M, Frankenberger WT. Influence of L-tryptophan and auxins applied to the rhizosphere on the vegetative growth of *Zea mays* L. Plant Soil. 1994;160:97–104.
3. Wongsuk T, Pumeesat P, Luplertlop N. Fungal quorum sensing molecules: role in fungal morphogenesis and pathogenicity. J Basic Microbiol. 2016;56:440–7.
4. Inagaki S, Morimura S, Gondo K, Tang Y, Akutagawa H, Kida K. Isolation of tryptophol as an apoptosis-inducing component of vinegar produced from boiled extract of black soybean in human monoblastic leukemia U937 cells. Biosci Biotechnol Biochem. 2007;71:371–9.
5. Kaur R, Kapoor Y, Manjal SK, Rawal RK, Kumar K. Diversity-oriented synthetic approaches for furoindoline: a review. Curr Org Synth. 2019;16:342–68.
6. Tfelt-Hansen P, De Vries P, Saxena PR. Triptans in migraine: a comparative review of pharmacology, pharmacokinetics and efficacy. Drugs. 2000;60:1259–87.
7. Pierce V, Shepperson NB, Todd MH, Waterfall JF. Investigation into the cardioregulatory properties of the α1-adrenoceptor blocker indoramin. Br J Pharmacol. 1986;87:433–41.
8. Bellamy N. Etodolac in the management of pain: a clinical review of a multipurpose analgesic. Inflammopharmacology. 1997;5:139–52.
9. Schiff PL. Ergot and its alkaloids. Am J Pharm Educ. 2006;70:98.
10. Mizutani M, Inagaki F, Nakanishi T, Yanagihara C, Tamai I, Mukai C. Total syntheses of (-)- and (+)-goniomitine. Org Lett. 2011;13:1796–9.
11. Bandini M, Eichholzer A. Catalytic functionalization of indoles in a new dimension. Angew Chemie - Int Ed. 2009;48:9608–44.
12. Bartoli G, Bencivenni G, Dalpozzo R. Organocatalytic strategies for the asymmetric functionalization of indoles. Chem Soc Rev. 2010;39:4449–65.
13. Chen JB, Jia YX. Recent progress in transition-metal-catalyzed enantioselective indole functionalizations. Org Biomol Chem. 2017;15:3550–67.
14. Dalpozzo R. Strategies for the asymmetric functionalization of indoles: an update. Chem Soc Rev. 2015;44:742–78.
15. Dubhashe YR, Sawant VM, Gaikar VG. Process intensification of continuous flow synthesis of tryptophol. Ind Eng Chem Res. 2018;57:2787–96.
16. Lv Y, Yu Z, Su W. A continuous kilogram-scale process for the manufacture of 7-ethyltryptophol. Org Process Res Dev. 2011;15:471–5.
17. Nikolau BJ, Perera MADN, Brachova L, Shanks B. Platform biochemicals for a biorenewable chemical industry. Plant J. 2008;54:536–45.
18. Adegboye MF, Ojuederie OB, Talia PM, Babalola OO. Bioprospecting of microbial strains for biofuel production: metabolic engineering, applications, and challenges. Biotechnol Biofuels. 2021;14:5.
19. Suástegui M, Shao Z. Yeast factories for the production of aromatic compounds: from building blocks to plant secondary metabolites. J Ind Microbiol Biotechnol. 2016;43:1611–24.
20. Gori K, Knudsen PB, Nielsen KF, Arneborg N, Jespersen L. Alcohol-based quorum sensing plays a role in adhesion and sliding motility of the yeast *Debaryomyces hansenii*. FEMS Yeast Res. 2011;11:643–52.
21. Rosazza JP, Juhl R, Davis P. Tryptophol formation by *Zygosaccharomyces priorianus*. Appl Microbiol. 1973;26:98–105.
22. Dickinson JR, Salgado LEJ, Hewlins MJE. The catabolism of amino acids to long chain and complex alcohols in *Saccharomyces cerevisiae*. J Biol Chem. 2003;278:8028–34.
23. Ghosh S, Kebaara BW, Atkin AL, Nickerson KW. Regulation of aromatic alcohol production in *Candida albicans*. Appl Environ Microbiol. 2008;74:7211–8.
24. Gong X, Luo H, Hong L, Wu J, Wu H, Song C, et al. Effects of tryptophan and phenylalanine on tryptophol production in *Saccharomyces cerevisiae* revealed by transcriptomic and metabolomic analyses. J Microbiol. 2022;60:832–42.
25. Hazelwood LA, Daran J-M, van Maris AJA, Pronk JT, Dickinson JR. The Ehrlich pathway for fusel alcohol production: a century of research on *Saccharomyces cerevisiae* metabolism. Appl Environ Microbiol. 2008;74:2259–66.
26. Brachmann CB, Davies A, Cost GJ, Caputo E, Li J, Hieter P, et al. Designer deletion strains derived from *Saccharomyces cerevisiae* S288C: a useful set of strains and plasmids for PCR-mediated gene disruption and other applications. Yeast. 1998;14:115–32.
27. Entian KD, Kötter P. 25 yeast genetic strain and plasmid collections. Methods Microbiol. 2007. https://doi.org/10.1016/S0580-9517(06)36025-4.
28. Lee ME, DeLoache WC, Cervantes B, Dueber JE. A highly characterized yeast toolkit for modular, multipart assembly. ACS Synth Biol. 2015;4:975–86.
29. Engler C, Kandzia R, Marillonnet S. A one pot, one step, precision cloning method with high throughput capability. PLoS ONE. 2008;3: e3647.

30. Engler C, Gruetzner R, Kandzia R, Marillonnet S. Golden gate shuffling: a one-pot DNA shuffling method based on type IIs restriction enzymes. PLoS ONE. 2009;2009(4):e5553.
31. Heckman KL, Pease LR. Gene splicing and mutagenesis by PCR-driven overlap extension. Nat Protoc. 2007;2:924–32.
32. Chan WT, Verma CS, Lane DP, Gan SKE. A comparison and optimization of methods and factors affecting the transformation of *Escherichia coli*. Biosci Rep. 2013;33: e00086.
33. Gietz RD, Schiestl RH. High-efficiency yeast transformation using the LiAc/SS carrier DNA/PEG method. Nat Protoc. 2007;2:31–4.
34. Li Y, Mensah EO, Fordjour E, Bai J, Yang Y, Bai Z. Recent advances in high-throughput metabolic engineering: Generation of oligonucleotide-mediated genetic libraries. Biotechnol Adv. 2022;59: 107970.
35. Liu Q, Yu T, Li X, Chen Y, Campbell K, Nielsen J, et al. Rewiring carbon metabolism in yeast for high level production of aromatic chemicals. Nat Commun. 2019;10:1–13.
36. Choi KR, Ryu JY, Lee SY. Revisiting statistical design and analysis in scientific research. Small. 2018;14: e1802604.
37. Suástegui M, Guo W, Feng X, Shao Z. Investigating strain dependency in the production of aromatic compounds in *Saccharomyces cerevisiae*. Biotechnol Bioeng. 2016;113:2676–85.
38. Suástegui M, Yu Ng C, Chowdhury A, Sun W, Cao M, House E, et al. Multilevel engineering of the upstream module of aromatic amino acid biosynthesis in *Saccharomyces cerevisiae* for high production of polymer and drug precursors. Metab Eng. 2017;42:134–44.
39. Rodriguez A, Chen Y, Khoomrung S, Özdemir E, Borodina I, Nielsen J. Comparison of the metabolic response to over-production of *p*-coumaric acid in two yeast strains. Metab Eng. 2017;44:265–72.
40. Bisquert R, Planells-Cárcel A, Valera-García E, Guillamón JM, Muñiz-Calvo S. Metabolic engineering of *Saccharomyces cerevisiae* for hydroxytyrosol overproduction directly from glucose. Microb Biotechnol. 2022;15:1499–510.
41. Guo D, Zhang L, Kong S, Liu Z, Li X, Pan H. Metabolic engineering of *Escherichia coli* for production of 2-phenylethanol and 2-phenylethyl acetate from glucose. J Agric Food Chem. 2018;66:5886–91.
42. Kang Z, Zhang C, Du G, Chen J. Metabolic engineering of *Escherichia coli* for production of 2-phenylethanol from renewable glucose. Appl Biochem Biotechnol. 2014;172:2012–21.
43. Liu H, Tian Y, Zhou Y, Kan Y, Wu T, Xiao W, et al. Multi-modular engineering of *Saccharomyces cerevisiae* for high-titre production of tyrosol and salidroside. Microb Biotechnol. 2021;14:2605–16.
44. Liu Y, Liu H, Hu H, Ng KR, Yang R, Lyu X. De novo production of hydroxytyrosol by metabolic engineering of *Saccharomyces cerevisiae*. J Agric Food Chem. 2022;70:7490–9.
45. Satoh Y, Tajima K, Munekata M, Keasling JD, Lee TS. Engineering of a tyrosol-producing pathway, utilizing simple sugar and the central metabolic tyrosine, in *Escherichia coli*. J Agric Food Chem. 2012;60:979–84.
46. Xu W, Yang C, Xia Y, Zhang L, Liu C, Yang H, et al. High-level production of tyrosol with noninduced recombinant *Escherichia coli* by metabolic engineering. J Agric Food Chem. 2020;68:4616–23.
47. Zhu L, Xu S, Li Y, Shi G. Improvement of 2-phenylethanol production in *Saccharomyces cerevisiae* by evolutionary and rational metabolic engineering. PLoS ONE. 2021;16: e0258180.
48. Koopman F, Beekwilder J, Crimi B, van Houwelingen A, Hall RD, Bosch D, et al. De novo production of the flavonoid naringenin in engineered *Saccharomyces cerevisiae*. Microb Cell Fact. 2012;11:155.
49. Luttik MAH, Vuralhan Z, Suir E, Braus GH, Pronk JT, Daran JM. Alleviation of feedback inhibition in *Saccharomyces cerevisiae* aromatic amino acid biosynthesis: quantification of metabolic impact. Metab Eng. 2008;10:141–53.
50. Trenchard IJ, Siddiqui MS, Thodey K, Smolke CD. De novo production of the key branch point benzylisoquinoline alkaloid reticuline in yeast. Metab Eng. 2015;31:74–83.
51. Graf R, Mehmann B, Braus GH. Analysis of feedback-resistant anthranilate synthases from *Saccharomyces cerevisiae*. J Bacteriol. 1993;175:1061–8.
52. Prasad R, Niederberger P, Hütter R. Tryptophan accumulation in *Saccharomyces cerevisiae* under the influence of an artificial yeast TRP gene cluster. Yeast. 1987;3:95–105.
53. Zhang J, Petersen SD, Radivojevic T, Ramirez A, Pérez-Manríquez A, Abeliuk E, et al. Combining mechanistic and machine learning models for predictive engineering and optimization of tryptophan metabolism. Nat Commun. 2020;11:4880.
54. Milne N, Thomsen P, Mølgaard Knudsen N, Rubaszka P, Kristensen M, Borodina I. Metabolic engineering of *Saccharomyces cerevisiae* for the de novo production of psilocybin and related tryptamine derivatives. Metab Eng. 2020;60:25–36.
55. Kuivanen J, Kannisto M, Mojzita D, Rischer H, Toivari M, Jäntti J. Engineering of *Saccharomyces cerevisiae* for anthranilate and methyl anthranilate production. Microb Cell Fact. 2021;20:34.
56. Walsh CT, Haynes SW, Ames BD. Aminobenzoates as building blocks for natural product assembly lines. Nat Prod Rep. 2012;29:37–59.
57. Luo ZW, Cho JS, Lee SY. Microbial production of methyl anthranilate, a grape flavor compound. Proc Natl Acad Sci USA. 2019;166:10749–56.
58. Iraqui I, Vissers S, Cartiaux M, Urrestarazu A. Characterisation of *Saccharomyces cerevisiae ARO8* and *ARO9* genes encoding aromatic aminotransferases I and II reveals a new aminotransferase subfamily. Mol Gen Genet. 1998;257:238–48.
59. Romagnoli G, Luttik MAH, Kötter P, Pronk JT, Daran JM. Substrate specificity of thiamine pyrophosphate-dependent 2-oxo-acid decarboxylases in *Saccharomyces cerevisiae*. Appl Environ Microbiol. 2012;78:7538–48.
60. De Smidt O, Du Preez JC, Albertyn J. The alcohol dehydrogenases of *Saccharomyces cerevisiae*: a comprehensive review. FEMS Yeast Res. 2008;8:967–78.
61. Lu H, Li F, Sánchez BJ, Zhu Z, Li G, Domenzain I, et al. A consensus *S. cerevisiae* metabolic model Yeast8 and its ecosystem for comprehensively probing cellular metabolism. Nat Commun. 2019;10:3586.
62. Heirendt L, Arreckx S, Pfau T, Mendoza SN, Richelle A, Heinken A, et al. Creation and analysis of biochemical constraint-based models using the COBRA Toolbox v.3.0. Nat Protoc. 2019;14:639–702.
63. Liu Q, Liu Y, Chen Y, Nielsen J. Current state of aromatics production using yeast: achievements and challenges. Curr Opin Biotechnol. 2020;65:65–74.
64. Thompson B, Machas M, Nielsen DR. Creating pathways towards aromatic building blocks and fine chemicals. Curr Opin Biotechnol. 2015;36:1–7.
65. Cao M, Gao M, Suástegui M, Mei Y, Shao Z. Building microbial factories for the production of aromatic amino acid pathway derivatives: From commodity chemicals to plant-sourced natural products. Metab Eng. 2020;58:94–132.
66. Chang MCY, Keasling JD. Production of isoprenoid pharmaceuticals by engineered microbes. Nat Chem Biol. 2006;2:674–81.
67. Jung ST, Lauchli R, Arnold FH. Cytochrome P450: taming a wild type enzyme. Curr Opin Biotechnol. 2011;22:809–17.
68. Cravens A, Payne J, Smolke CD. Synthetic biology strategies for microbial biosynthesis of plant natural products. Nat Commun. 2019;10:2142.
69. Kotopka BJ, Li Y, Smolke CD. Synthetic biology strategies toward heterologous phytochemical production. Nat Prod Rep. 2018;35:902–20.
70. Li S, Li Y, Smolke CD. Strategies for microbial synthesis of high-value phytochemicals. Nat Chem. 2018;10:395–404.
71. Curran KA, Leavitt JM, Karim AS, Alper HS. Metabolic engineering of muconic acid production in *Saccharomyces cerevisiae*. Metab Eng. 2013;15:55–66.
72. Galanie S, Thodey K, Trenchard IJ, Interrante MF, Smolke CD. Complete biosynthesis of opioids in yeast. Science. 2015;349:1095–100.
73. Liu H, Wu X, Ma H, Li J, Liu Z, Guo X, et al. High-level production of hydroxytyrosol in engineered *Saccharomyces cerevisiae*. ACS Synth Biol. 2022;11:3706–13.
74. Brown S, Clastre M, Courdavault V, O'Connor SE. De novo production of the plant-derived alkaloid strictosidine in yeast. Proc Natl Acad Sci U S A. 2015;112:3205–10.
75. Zhang J, Hansen LG, Gudich O, Viehrig K, Lassen LMM, Schrübbers L, et al. A microbial supply chain for production of the anti-cancer drug vinblastine. Nature. 2022;609:341–7.
76. Zhang J, Wu C, Sheng J, Feng X. Molecular basis of 5-hydroxytryptophan synthesis in *Saccharomyces cerevisiae*. Mol Biosyst. 2016;12:1432–5.
77. Germann SM, Baallal Jacobsen SA, Schneider K, Harrison SJ, Jensen NB, Chen X, et al. Glucose-based microbial production of the hormone melatonin in yeast *Saccharomyces cerevisiae*. Biotechnol J. 2016;11:717–24.
78. Milne N, Sáez-sáez J, Nielsen M, Dyekjær D. Engineering *Saccharomyces cerevisiae* for the de novo production of halogenated tryptophan and tryptamine derivatives. ChemistryOpen. 2023;12: e202200266.

79. Pyne ME, Narcross L, Melgar M, Kevvai K, Mookerjee S, Leite GB, et al. An engineered Aro1 protein degradation approach for increased cis, cis-muconic acid biosynthesis in *Saccharomyces cerevisia*e. Appl Environ Microbiol. 2018;84:e01095-e1118.
80. Reifenrath M, Boles E. Engineering of hydroxymandelate synthases and the aromatic amino acid pathway enables de novo biosynthesis of mandelic and 4-hydroxymandelic acid with *Saccharomyces cerevisiae*. Metab Eng. 2018;45:246–54.
81. Rodriguez A, Kildegaard KR, Li M, Borodina I, Nielsen J. Establishment of a yeast platform strain for production of p-coumaric acid through metabolic engineering of aromatic amino acid biosynthesis. Metab Eng. 2015;31:181–8.
82. Chen Y, Li F, Nielsen J. Genome-scale modeling of yeast metabolism: retrospectives and perspectives. FEMS Yeast Res. 2022;22:1–9.

Publisher's Note